JOURNAL OF MATERIALS SCIENCE 29 (1994) 5541–5550

Interfacial debonding and fibre pull-out stresses

Part V *A methodology for evaluation of interfacial properties*

LI-MIN ZHOU, YIU-WING MAI*, CAROLINE BAILLIE
Centre for Advanced Materials Technology, Department of Mechanical and Mechatronic Engineering, University of Sydney, Sydney, NSW 2006, Australia

Based on a theoretical model developed previously by the authors in Part II of this series for a single fibre pull-out test, a methodology for the evaluation of interfacial properties of fibre–matrix composites is presented to determine the interfacial fracture toughness G_c, the friction coefficient μ, the radial residual clamping stress q_0 and the critical bonded fibre length z_{max}. An important parameter, the stress drop $\Delta\sigma$, which is defined as the difference between the maximum debond stress σ_d^* and the initial frictional pull-out stress σ_{fr}, is introduced to characterize the interfacial debonding and fibre pull-out behaviour. The maximum logarithmic stress drop, $\ln(\Delta\sigma)$, is obtained when the embedded fibre length L is equal to the critical bonded fibre length z_{max}. The slope of the $\ln(\Delta\sigma)$–L curve for L bigger than z_{max} is found to be a constant that is related to the interfacial friction coefficient μ. The effect of fibre anisotropy on fibre debonding and fibre pull-out is also included in this analysis. Published experimental data for several fibre–matrix composites are chosen to evaluate their interfacial properties by using the present methodology.

1. Introduction

The properties of the fibre–matrix interface are now widely recognized as having a significant effect on the physical and mechanical behaviour of fibre-reinforced composites [1–7]. The realization of the importance of interfacial properties always requires proper characterization of the interface in terms of both experiments and micromechanics. However, the tailoring of interfacial properties to optimize composite performance is still far from being a matured science. A common problem lies in the incomplete identification of the various parameters which may be significant. Much work has already been done to evaluate the interfacial properties of various fibre composite systems. These properties include the interfacial fracture toughness G_c (or interfacial shear strength τ_s), the coefficient of friction μ and the thermal residual clamping stress q_0. Several experimental techniques based on single-fibre pull-out or push-out have been developed and successfully used to measure the load–displacement curve which can give the maximum debond and frictional pull-out or push-out stresses. Many relevant analytical models have also been established, based primarily on shear-lag analysis to provide a theoretical framework for experimental evaluation of the interfacial properties.

Recently, a series of theoretical and experimental studies of the fibre pull-out problem have been performed by the authors for a single fibre-reinforced elastic matrix composite [8–11]. In Part II of this series [9] an improved analysis was developed for an isotropic fibre–matrix composite, based on the concept of fracture mechanics where the debonded region was considered as an interfacial crack and its extension was dependent on a fracture energy criterion being satisfied. Poisson contraction of the fibre when subjected to tension was also included, which resulted in a generalized non-uniform friction along the debonded region. Solutions for the partial debond stress σ_d^p during progressive debonding, and the initial frictional pull-out stress σ_{fr} after complete debonding, were derived which were related to the material constants, the geometric factors of the composite constituents and the interfacial properties. However, the procedure to evaluate the interfacial properties was not given.

The purpose of the present study is to provide a methodology, on the basis of the theoretical model developed in Part II [9], to determine the interfacial properties of the fibre–matrix composites. A stress drop analysis is presented to characterize the behaviour of fibre–matrix interface debonding and fibre pull-out. The effect of fibre anisotropy is also considered in this work.

2. Theory

2.1. Governing equations

The geometry of the fibre–matrix cylindrical model used in the previous study [8–10] is shown in Fig. 1. A single fibre with radius a is embedded at the centre of a coaxial cylindrical shell of the matrix with a radius b and a total length L. A set of cylindrical coordinates (r, θ, z) is selected so that the z-axis corresponds to the

* On leave at the Department of Mechanical Engineering, Hong Kong University of Science and Technology, Clear Water Bay, Hong Kong.

0022–2461

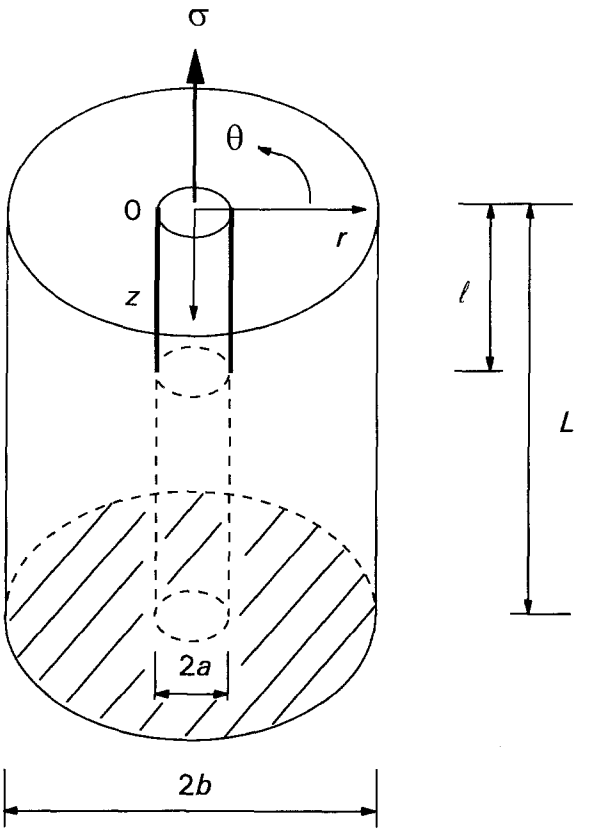

Figure 1 Schematic diagram of the fibre pull-out model.

axis of the fibre and r is the distance from the fibre axis. A partial debonded region of length l is initially given at the free fibre end. In a single-fibre pull-out test, a tensile stress is applied to the fibre end at $z = 0$ and the matrix is fixed at $z = L$. The model of deformations is symmetric about the fibre axis (i.e. axisymmetric) and thus the stress components (σ^r, σ^θ, σ^z, τ^{rz}) and the displacement components (u^r, u^z) are all independent of the tangential coordinate θ. In this analysis, the fibre is treated as a transversely isotropic elastic material and the matrix is isotropic. To simplify the analysis it is assumed that the fibre has a precisely cylindrical shape, so that the effects of surface roughness do no arise; the axial stresses in the fibre and the matrix are taken as the average of the fibre and the matrix stresses in the r-direction [3, 4, 9], respectively, i.e.

$$\sigma_f^z(z) = \frac{2}{a^2}\int_0^a \sigma_f^z(r,z)r\,dr \quad (1)$$

$$\sigma_m^z(z) = \frac{2\gamma}{a^2}\int_a^b \sigma_m^z(r,z)r\,dr \quad (2)$$

where $\gamma = a^2/(b^2 - a^2)$ is the volume ratio of the fibre to the matrix. The subscripts f and m refer to fibre and matrix and the superscripts are coordinate directions. The complete solutions of the stress distribution for an isotropic fibre and matrix have been derived previously in Part II [9]. The basic governing equations and the procedure used in deriving solutions for composites with a transversely isotropic fibre are similar to those with an isotropic fibre and are summarized below. When an axial stress is applied at the fibre end ($z = 0$), the stress transfers from the fibre to the matrix through the interfacial shear stress $\tau(z)$. The mechanical equilibrium conditions between fibre, matrix and interface require that

$$\sigma = \sigma_f^z(z) + \frac{1}{\gamma}\sigma_m^z(z) \quad (3)$$

$$\frac{d\sigma_f^z(z)}{dz} = -\frac{2}{a}\tau(z) \quad (4)$$

$$\frac{d\sigma_m^z(z)}{dz} = \frac{2\gamma}{a}\tau(z) \quad (5)$$

$$r\frac{\partial\sigma_m^z(z)}{\partial z} + \frac{\partial r\tau_m^{rz}(r,z)}{\partial r} = 0 \quad (6)$$

where $\tau(z)$ represents the interfacial frictional shear stress $\tau_f(z)$ in the debonded region and the interfacial shear stress $\tau_i(z)$ in the bonded region. For a transversely isotropic fibre and and isotropic matrix, the general relationships between strains ε and stresses σ are given by

$$\varepsilon_f^z(r,z) = \frac{1}{E_f}[\sigma_f^z(z) - 2\nu_f q_a(z)] \quad (7)$$

$$\varepsilon_f^\theta(r,z) = \frac{1}{E_f^r}(1 - \nu_f^r)q_a(z) - \frac{1}{E_f}\nu_f\sigma_f^z(z) \quad (8)$$

$$\varepsilon_m^z(r,z) = \frac{1}{E_m}[\sigma_m^z(z) + 2\gamma\nu_m q_a(z)] \quad (9)$$

$$\varepsilon_m^\theta(r,z) = \frac{\gamma}{E_m}\left[\nu_m\left(1 - \frac{b^2}{r^2}\right) - 1 - \frac{b^2}{r^2}\right]q_a - \frac{1}{E_m}\nu_m\sigma_m^z(z) \quad (10)$$

$$\varepsilon_m^{rz} = \frac{1}{2}\left(\frac{\partial u_m^z(r,z)}{\partial r}\right) = \frac{2(1 + \nu_m)}{E_f}\tau_m^{rz}(r,z) \quad (11)$$

where E and ν represent Young's modulus and Poisson's ratio, respectively. ν_f^r and E_f^r are the Poisson's ratio and Young's modulus in the plane perpendicular to the fibre axis. $q_a(z)$ is the interfacial radial tensile stress between fibre and matrix. In Equation 11 for the matrix shear strain, the radial displacement gradient with respect to the z-direction is neglected when compared to the axial displacement gradient with respect to the r-direction.

2.2. Stress components in constituents

In the debonded region ($0 \le z \le l$), frictional slip occurs at the interface where the stress transfer is assumed to satisfy the Coulomb friction law for a constant coefficient of friction μ:

$$\tau_f = -\mu(q_0 + q_a) \quad (12)$$

where q_0 is the residual clamping stress (compressive) caused by the matrix shrinkage and differential thermal contraction of the constituents. The interfacial radial stress $q_a(z)$ arising from Poisson contraction between the fibre and the matrix can be obtained by using the condition that they must remain in contact during sliding so that continuity of the tangential

strains at the interface holds and $\varepsilon_f^\theta(a,z) = \varepsilon_m^\theta(a,z)$, i.e.

$$q_a = \frac{\alpha\nu_f\sigma_f^z(z) - \nu_m\sigma_m^z(z)}{\alpha_1(1-\nu_f^r) + 2\gamma + 1 + \nu_m} \quad (13)$$

where $\alpha = E_m/E_f$ and $\alpha_1 = E_m/E_f^r$ are the ratios of Young's moduli. Further, the shear stress in the matrix $\tau_m^{rz}(r,z)$ is expressed as a function of $\tau(z)$ for the boundary conditions that the stresses are compatible at the interface, i.e. $\tau_m^{rz}(a,z) = \tau(z)$, and the stress is zero at the outer surface of the matrix (i.e. $\tau_m^{rz}(b,z) = 0$) at both the debonded and bonded regions. The axial fibre stress at the fibre end is equal to the applied stress (i.e. $\sigma_f^z(0) = \sigma$) and the matrix is stress-free (i.e. $\sigma_m^z(0) = 0$). In the bonded region ($l \le z \le L$), the no-slip condition at the interface $u_f^z(a,z) = u_m^z(a,z)$ is used to drive the differential equation for the axial fibre stress. Therefore, solving the above equations with given boundary conditions, the stress distributions in the fibre and matrix and at the interface are given for the debonded region ($0 \le z \le l$) by

$$\sigma_f^z(z) = \sigma - \omega(\bar{\sigma} - \sigma)[\exp(\lambda z) - 1] \quad (14)$$

$$\sigma_m^z(z) = \gamma\omega(\bar{\sigma} - \sigma)[\exp(\lambda z) - 1] \quad (15)$$

$$\tau_m^{rz}(r,z) = \lambda\gamma\omega(\bar{\sigma} - \sigma)\frac{(b^2 - r^2)\exp(\lambda z)}{2r} \quad (16)$$

$$\tau_f(z) = \frac{a\lambda\omega}{2}(\bar{\sigma} - \sigma)\exp(\lambda z) \quad (17)$$

where

$$\omega = \frac{\alpha\nu_f}{\alpha\nu_f + \gamma\nu_m} \quad (18)$$

$$k = \frac{\alpha\nu_f + \gamma\nu_m}{\alpha_1(1-\nu_f^r) + 1 + \nu_m + 2\gamma} \quad (19)$$

λ and $\bar{\sigma}$ are the reciprocal friction length and the asymptotic debond stress, respectively, and are given by

$$\lambda = 2\mu k/a \quad (20)$$

$$\bar{\sigma} = -q_0/\omega k \quad (21)$$

Also, the solutions for the bonded region ($0 \le z \le l$) are obtained as

$$\sigma_f^z(z) = \frac{(\eta\sigma + \sigma_l)\sinh[A_1^{1/2}(L-z)] - \eta\sigma\sinh[A_1^{1/2}(l-z)]}{\sinh[A_1^{1/2}(L-l)]} - \eta\sigma \quad (22)$$

$$\sigma_m^z(z) = \gamma(1+\eta)\sigma - \gamma\frac{(\eta\sigma + \sigma_l)\sinh[A_1^{1/2}(L-z)] - \eta\sigma\sinh[A_1^{1/2}(l-z)]}{\sinh[A_1^{1/2}(L-l)]} \quad (23)$$

$$\tau_m^{rz}(r,z) = \frac{\gamma A_1^{1/2}(b^2 - r^2)\{(\eta\sigma + \sigma_l)\cosh[A_1^{1/2}(L-z)] - \eta\sigma\cosh[A_1^{1/2}(l-z)]\}}{2r\sinh[A_1^{1/2}(L-l)]} \quad (24)$$

$$\tau_i(z) = \frac{aA_1^{1/2}\{(\eta\sigma + \sigma_l)\cosh[A_1^{1/2}(L-z)] - \eta\sigma\cosh[A_1^{1/2}(l-z)]\}}{2\sinh[A_1^{1/2}(L-l)]} \quad (25)$$

where

$$A_1 = \frac{\gamma(2k\nu_m - 1)}{\eta(1+\nu_m)[2\gamma b^2\ln(b/a) - a^2]} \quad (26)$$

$$\eta = \frac{\gamma(2k\nu_m - 1)}{\alpha(1 - 2k\nu_f) + \gamma(1 - 2k\nu_m)} \quad (27)$$

σ_l is the crack tip debond stress at the boundary between debonded and bonded regions at $z = l$ and is determined by the continuity condition of the fibre axial stress:

$$\sigma_l = \sigma - \omega(\bar{\sigma} - \sigma)[\exp(\lambda l) - 1] \quad (28)$$

2.3. Interfacial debonding criterion

To establish the relationship between the debonding stress and the debonding length during fibre pull-out, the fracture mechanics approach is used to derive an interface debond criterion where the strain energy release rate against the incremental debond length is equated to the interfacial fracture toughness G_c, which is considered as a material constant:

$$2\pi a G_c = \frac{\partial U_t}{\partial l} \quad (29)$$

where U_t is the total elastic strain energy stored in the fibre and the matrix in both debonded and bonded regions and is obtained by integrating the stress components acting in the constituents over the volume of the respective regions:

$$U_t = \int_0^L\int_0^b\left[\frac{\sigma_f(z)^2}{E_f} + \frac{\sigma_m(z)^2}{E_m} + \frac{2(1+\nu_m)\tau_m(r,z)^2}{E_m}\right]\pi r dr dz \quad (30)$$

Substituting the solutions for the three major stress components σ_f, σ_m and τ_m determined in the debonded and bonded regions into Equation 30, the fibre–matrix interface debond criterion is derived as

$$G_c = \frac{1}{2\pi a}[B\sigma^2 + C(\bar{\sigma} - \sigma)\sigma + D(\bar{\sigma} - \sigma)^2] \quad (31)$$

in which the coefficients B, C and D are complex functions of material properties of the constituents and geometric factors, and are given by Equations A9, A10 and A11, respectively, in part II [9].

3. Parametric study and discussion

3.1. Debonding and frictional pull-out stresses

A typical load–displacement diagram for a single-fibre pull-out test is shown in Fig. 2. Upon loading, there is an initial linear relationship until initial debonding

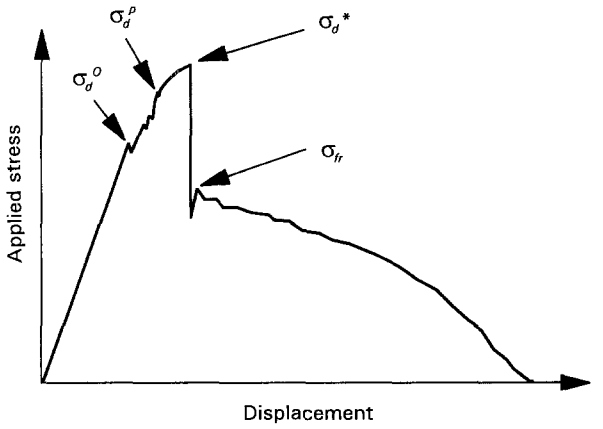

Figure 2 Schematic diagram of the stress–displacement curve for a single-fibre pull-out test. Subscripts d and fr are for debond and friction. Superscripts 0, p and * are for initial, partial and maximum stresses, respectively.

occurs at σ_d^0. This debond stress increases steadily to a maximum value σ_d^* and then drops to an initial frictional pull-out stress σ_{fr} at which time debonding is complete along the fibre–matrix interface. Therefore, the applied stress σ in the debond criterion (Equation 31) may represent the initial debonding stress σ_d^0, the partial debonding stress σ_d^p, the maximum debonding stress σ_d^* and the complete debonding stress (or initial frictional pull-out) σ_{fr}, respectively, depending on the different stages of the interfacial debonding process.

From the force balance condition of the fibre in the debonded region, the partial debonding stress can be written as the sum of the crack tip debond stress and the stress component due to friction, i.e.

$$\sigma_d^p = \sigma_l + \frac{2}{a}\int_0^l \tau_f \, dz \tag{32}$$

Substituting Equation 17 into Equation 32 gives

$$\sigma_d^p = \sigma_l + (\bar{\sigma} - \sigma_l)\frac{\omega[\exp(\lambda l) - 1]}{1 + \omega[\exp(\lambda l) - 1]} \tag{33}$$

When the debond length reaches the embedded fibre length, i.e. $l = L$, the crack tip debond stress becomes zero and the initial frictional pull-out stress is obtained from Equation 33 as

$$\sigma_{fr} = \omega\bar{\sigma}\frac{[\exp(\lambda L) - 1]}{1 + \omega[\exp(\lambda L) - 1]} \tag{34}$$

In many fibre pull-out tests $b \gg a$, $\omega \simeq l$ and Equations 33 and 34 are simplified respectively to

$$\sigma_d^p = \sigma_l + (\bar{\sigma} - \sigma_l)[1 - \exp(-\lambda l)] \tag{35}$$

$$\sigma_{fr} = \bar{\sigma}[1 - \exp(-\lambda L)] \tag{36}$$

To illustrate the variations of the applied stress with the characteristic lengths of the composite system (i.e. partial debonding length l and embedded fibre length L) during fibre pull-out, specific results are calculated based on the solutions presented in the previous sections for three different model composites, i.e. release-agent coated steel wire–epoxy matrix [8], carbon fibre–epoxy matrix [8] and untreated SiC fibre–borosilicate glass matrix [12] whose material constant and geometric factors are shown in Table I.

TABLE I Material constants and geometric factors for several fibre–matrix composites

Composite system	Material constants				Radii	
	E_f (GPa)	E_m (GPa)	v_f	v_m	a (mm)	b (mm)
Coasted steel wire–epoxy matrix [8]	179	2.98	0.3	0.35	0.275	6.5
Carbon fibre–epoxy matrix [8]	230	3.0	0.2	0.4	0.003	1.0
Untreated SiC fibre–glass matrix [12]	400	70	0.17	0.2	0.071	2.8
Steel wire–epoxy matrix [14]	173	3.72	0.35	0.39	0.075	3.0

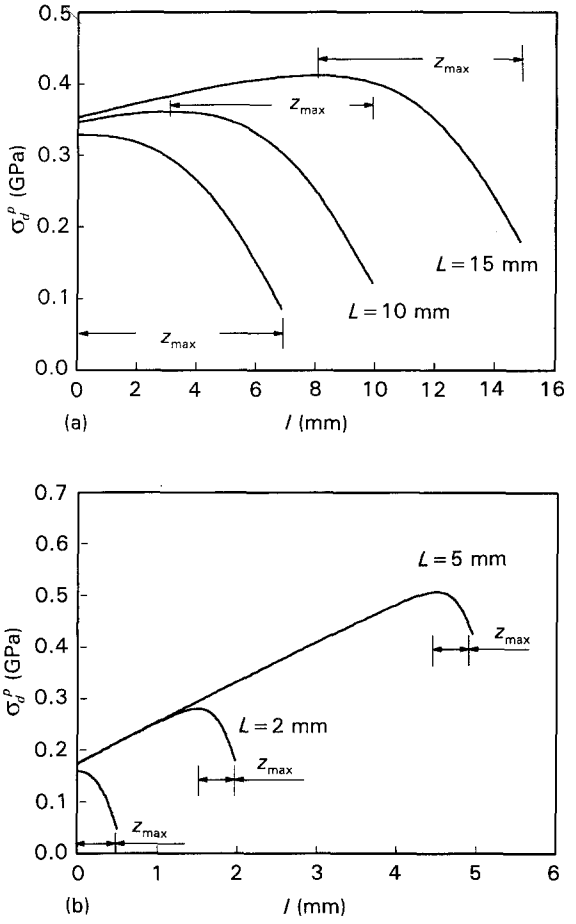

Figure 3 Plots of partial debond stress σ_d^p as a function of debond length l for different embedded fibre length L: (a) release-agent coated steel wire–epoxy matrix composite [8] ($\mu = 0.22$, $q_0 = -7.28$ MPa, $G_c = 34.7\ J\,m^{-2}$) and (b) untreated SiC fibre–borosilicate glass matrix composite [12] ($\mu = 0.048$, $q_0 = -64.5$ MPa, $G_c = 0.964\ J\,m^{-2}$).

According to Equation 35, the partial debonding stress is calculated and plotted as a function of debonding length for several total embedded fibre lengths as shown in Fig. 3 for the release-agent coated steel wire–epoxy matrix composite [8] (Fig. 3a) and an untreated SiC fibre–borosilicate glass matrix composite [12] (Fig. 3b, respectively. These two composite

systems are chosen for their typical interfacial properties (see captions of figures), namely a strong chemical bond in the epoxy matrix composite and a mechanical bond in the ceramic matrix composite. In general, the partial debonding stress σ_d^0 increases stably as the debond crack propagates, but it decreases after reaching a maximum value σ_d^* where the remaining bonded fibre length $L - l$ is equal to z_{max}. If the embedded fibre length L is smaller than or equal to z_{max}, the debond process is totally unstable and initial debonding leads immediately to complete debonding. Consequently, the maximum debond stress is determined simply after the debond crack is initiated (i.e. $\sigma_d^0 = \sigma_d^*$).

The maximum debond stress σ_d^*, the crack tip debond σ_l at $l = L - z_{max}$ and the frictional pull-out stress σ_{fr}, calculated based on Equations 35, 28 and 36, respectively, are plotted against embedded fibre length L in Fig. 4 for the release-agent coated stainless steel wire–epoxy matrix composite [8] (Fig. 4a) and the untreated SiC fibre–borosilicate glass matrix composite [12] (Fig. 4b). It is indicated that when $L < z_{max}$, the maximum debond stress is identical to the crack tip debond stress, i.e. $\sigma_d^* = \sigma_l$. Both σ_d^* and σ_l increase more rapidly than the initial frictional pull-out stress σ_{fr} with increasing embedded fibre length. If $L > z_{max}$, σ_d^* increases towards an asymptotic value $\bar{\sigma}$ but σ_l is almost invariant with L.

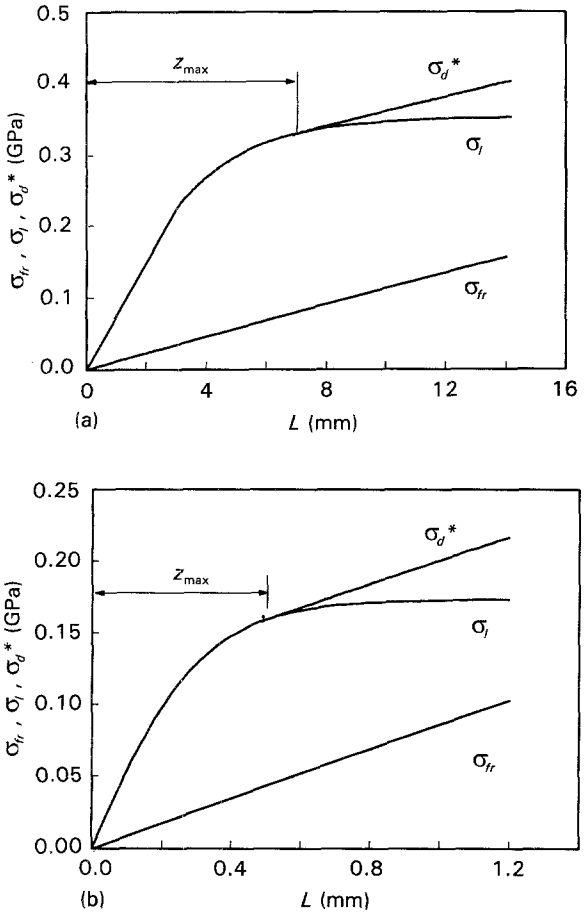

Figure 4 Plots of maximum debond stress σ_d^*, crack tip debond stress σ_l and initial frictional pull-out stress σ_{fr} against embedded fibre length L: (a) release-agent coated steel wire–epoxy matrix composite and (b) untreated SiC fibre–borosilicate glass matrix composite. For interfacial properties of these two composites refer to Fig. 3.

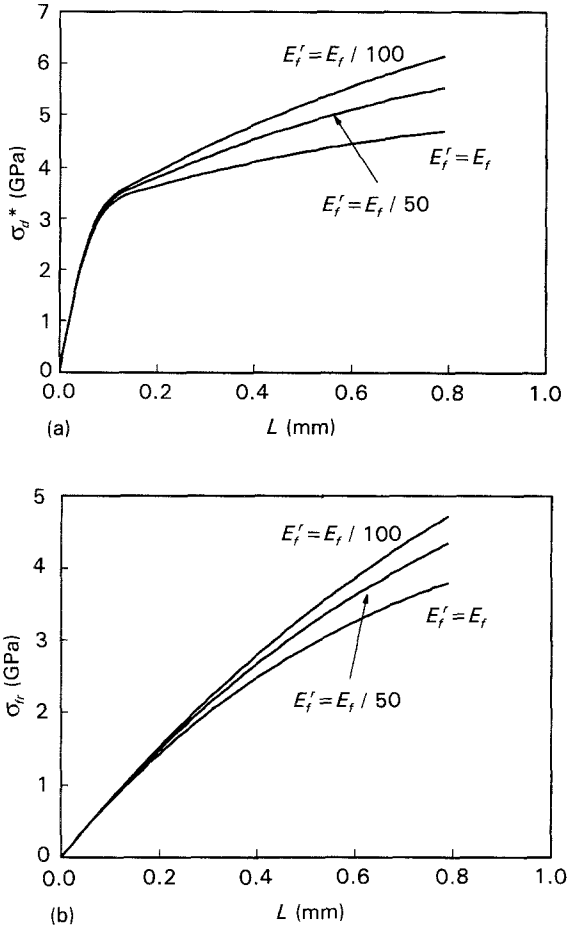

Figure 5 Plots of (a) maximum debond stress σ_d^* and (b) initial frictional pull-out stress σ_{fr} against embedded fibre length L, showing the effect of fibre anisotropy for a carbon fibre–epoxy matrix composite [8] ($\mu = 1.25$, $q_0 = -9.97$ MPa, $G_c = 37.7\ J\,m^{-2}$, $z_{max} = 0.145$ mm).

The above calculations are based on the isotropic properties of both fibre and matrix. However, it is realized that fibres used in advanced composites are often not isotropic. Usually, the elastic modulus is stiffer in the longitudinal direction than in the transverse direction. Similarly, the Poisson's ratios are not identical. To illustrate the effect of fibre anisotropy during fibre pull-out, the maximum debond stresses σ_d^*, calculated based on Equation 35 for different fibre transverse Young's moduli $E_f^r (= E_f, E_f/50, E_f/100)$ are plotted against the embedded fibre length L for the carbon fibre–epoxy matrix composite in Fig. 5a. The Poisson's ratio ν_f^r used in the calculations is the same as ν_f, i.e. $\nu_f^r = \nu_f$. It is clearly shown that as the fibre transverse Young's modulus E_f^r increases, the maximum debond stress increases for a given embedded fibre length. This trend is particularly obvious at large embedded fibre lengths. Similar results for the initial frictional pull-out stress σ_{fr} calculated from Equation 36 are shown in Fig. 5b. These results are attributed principally to the change in radial constraint at the interface resulting from Poisson contraction of the fibre when the transverse Young's modulus changes.

3.2. Critical bonded fibre length z_{max}

As discussed previously in Part I [8] and Part II [9] of

this paper and indicated in Fig. 4, the condition for unstable debonding requires that the derivative of the partial debond stress with respect to the debond length is equal to or less than zero, i.e.

$$\frac{\partial \sigma_d^p}{\partial l} \leq 0 \tag{37}$$

It is shown in Fig. 4 that for a given composite system the stability of the debond process depends on the partial debond length l relative to the embedded fibre length L and there is a critical bonded fibre length $z_{max}(= L - l)$ below which the debond process is always unstable. Accordingly, the instability condition (Equation 37) requires that for long embedded fibre lengths ($L \geq z_{max}$) the debond process becomes unstable when the slope of the σ_d^p–l curve is zero where the maximum debond stress σ_d^* is obtained. Alternatively, for short embedded fibre lengths ($L < z_{max}$), total unstable debonding occurs right from the beginning of the debonding process since the slope of σ_d^p–l curve is negative. It is unable to yield a closed-form solution of the critical bonded fibre length z_{max} because the partial debond stress σ_d^p is a complex function of the embedded fibre length as well as the partial debond length. However, if z^* is defined as a minimum fibre bonded length for stable debonding, the relation between z^* and L can be solved numerically from Equation 31 (or Equation 35) by determining the maximum debond stress which appears at $L - l = z^*$. Fig. 6 shows the minimum bonded fibre length z^* plotted against the embedded fibre length L for the release agent coated stainless steel wire–epoxy matrix (Fig. 6a) and the untreated SiC fibre–borosilicate glass matrix (Fig. 6b) composites. It is worth noticing that when the embedded fibre length L is shorter than the critical bonded fibre length z_{max}, the minimum bonded fibre length z^* varies linearly with L as $z^* = L$; and if the embedded fibre length L is longer than z_{max}, the minimum bonded fibre length z^* becomes a constant z_{max}. This implies that for a given composite system the critical bonded fibre length z_{max} is independent of the embedded fibre length L.

If a simplified solution for the partial debond stress proposed by Karbhari and Wilkins [13] is used, neglecting the effect of Poisson contraction of the fibre and assuming a constant frictional shear stress τ_f at the debonded region in the context of the maximum shear strength criterion, the above instability condition gives a closed-form solution from the critical bonded fibre length z_{max}:

$$z_{max} = \frac{l}{g}\cosh^{-1}\left[\frac{\tau_b}{\tau_f}\left(1 + \frac{\gamma}{\alpha}\right)\right]^{1/2} \tag{38}$$

where

$$g = \left(\frac{\alpha + \gamma}{\eta(1 + \nu_m)[\gamma b^2 \ln(b/a) - (a^2/2)]}\right)^{1/2} \tag{39}$$

It is obvious from Equation 38 that z_{max} depends on the interfacial properties and the material constants of the constituents. However, in the more rigorous fracture mechanics approach used in this work a closed form solution for z_{max} is not available. The technique to determine the interfacial properties of fibre–matrix composites is given in the next section.

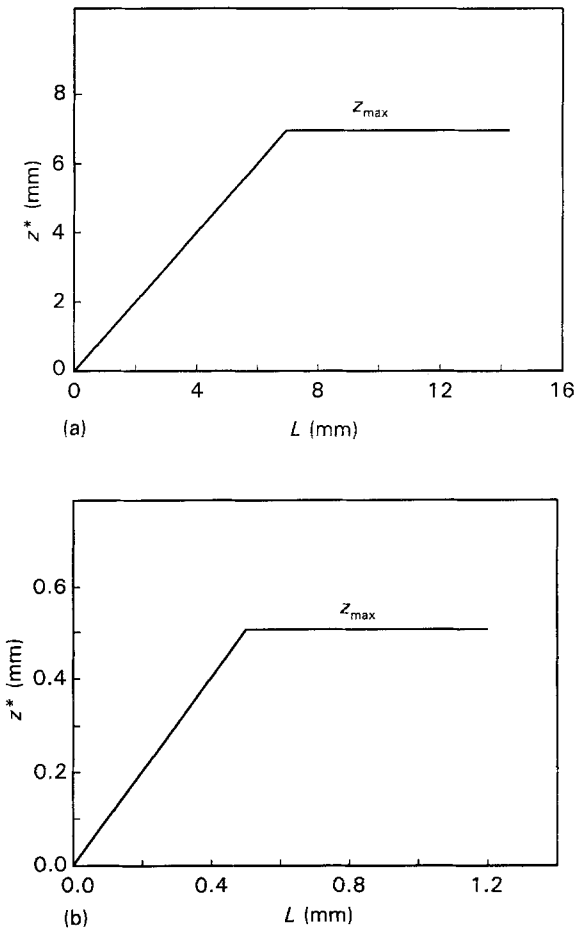

Figure 6 Plots of minimum bonded fibre length for stable debonding z^* as a function of embedded fibre length L: (a) release-agent coated steel wire–epoxy matrix composite and (b) untreated SiC fibre–borosilicate glass matrix composite. For interfacial properties of these two composites refer to Fig. 3.

4. Method for evaluation of the interfacial properties

Maximum debond stress σ_d^* and initial frictional pull-out stress σ_{fr} are usually measured from the applied stress–displacement curve (Fig. 2) for the different embedded fibre lengths L in fibre pull-out tests. These experimental data can be used to calculate the interfacial properties by matching the experimental data and the theoretical model. However, it is difficult to directly apply Equations 35 and 36 to determine four unknown parameters (i.e. μ, q_0, G_c and z_{max}), even by regression, because σ_d^* is a complex function of the partial debond length as well as embedded fibre length. To establish a simple method for the evaluation of interfacial properties on the basis of the present model, a stress drop analysis is developed as follows.

4.1. Stress drop analysis

As mentioned earlier, the maximum debond stress σ_d^* is obtained when the remaining bonded length, $L - l$, reaches a critical value z_{max} (or σ_d^* is determined

at the initial debond propagation if the embedded fibre length is shorter than the critical bonded length z_{max}). From Equation 35, σ_d^* is given by

$$\sigma_d^* = \sigma_l + (\bar{\sigma} - \sigma_l)\{1 - \exp[-\lambda(L - z^*)]\} \quad (40)$$

where the crack tip debond stress σ_l is determined at $l = L - z^*$. After the maximum debond stress is reached the partial debond stress decreases rapidly to the complete debond stress (or initial frictional pull-out stress) as shown in Fig. 3. Corresponding to this unstable debonding process, a stress drop is observed and recorded by the stress–displacement curve in the fibre pull-out experiment (see Fig. 2). By using Equations 35 and 36 the stress drop $\Delta\sigma$, which is the difference between the maximum debond stress σ_d^* and the initial frictional pull-out stress σ_{fr}, is obtained from

$$\begin{aligned}\Delta\sigma &= \sigma_d^* - \sigma_{fr} \\ &= \exp[-\lambda(L - z^*)] \\ &\quad \times \{\sigma_l + \bar{\sigma}[\exp(-\lambda z^*) - 1]\}\end{aligned} \quad (41)$$

Further, taking the logarithm of both sides gives

$$\begin{aligned}\ln(\Delta\sigma) &= -\lambda(L - z^*) \\ &\quad + \ln\{\sigma_l + \bar{\sigma}[\exp(-\lambda z^*) - 1]\}\end{aligned} \quad (42)$$

The logarithmic stress drop $\ln(\Delta\sigma)$ calculated from Equation 42 is plotted against the embedded fibre length L as shown in Fig. 7 for the carbon fibre–epoxy matrix composite studied in Part I [8]. It is seen that as the embedded fibre length increases from a very small value, $\ln(\Delta\sigma)$ increases non-linearly until it reaches a maximum value. After the maximum logarithmic stress drop is obtained, $\ln(\Delta\sigma)$ decreases linearly with L. According to the discussions in section 3.2, it is known that z_{max} is independent of embedded fibre length when $L > z_{max}$ (Fig. 6) and the crack tip debond stress σ_l becomes almost a constant (Fig. 4). Therefore, differentiating Equation 42 with respect to L yields

$$\frac{d}{dL}[\ln(\Delta\sigma)] = -\lambda < 0 \qquad L > z_{max} \quad (43)$$

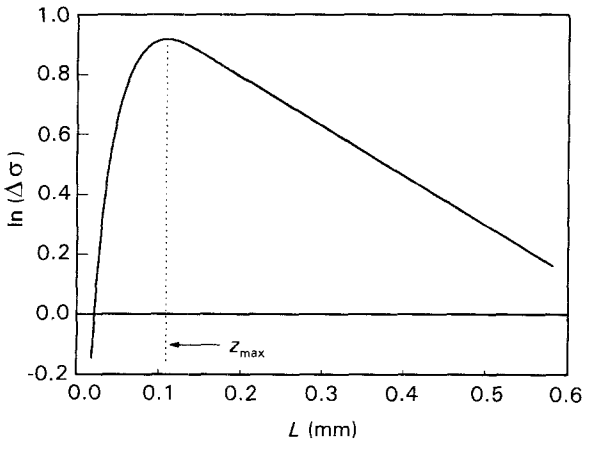

Figure 7 Plots of logarithmic stress drop $\ln(\Delta\sigma)$ as a function of embedded fibre length L for a carbon fibre–epoxy matrix composite [8] ($\mu = 1.25$, $q_0 = -9.97$ MPa, $G_c = 37.7\ J\,m^{-2}$).

Equation 43 means that when the embedded fibre length is longer than the critical bonded fibre length z_{max}, the slope of the $\ln(\Delta\sigma)$–L curve is always negative and equal to $-\lambda$ which is related to the interfacial friction coefficient μ by Equation 20. For smaller embedded fibre lengths, i.e. $0 < L < z_{max}$, $\sigma_l = \sigma_d^*$ and $z^* = L$ (Fig. 6). In this case it can be shown that

$$\begin{aligned}\frac{d}{dL}[\ln(\Delta\sigma)] &= \frac{1}{\sigma_d^* + \bar{\sigma}[\exp(-\lambda L) - 1]} \\ &\quad \times \left(\frac{d\sigma_d^*}{dL} - \lambda\bar{\sigma}\exp(-\lambda L)\right)\end{aligned} \quad (44)$$

From Equation 36 it is noted that

$$\begin{aligned}\frac{d\sigma_{fr}}{dL} &= \frac{d}{dL}\left\{\bar{\sigma}[1 - \exp(-\lambda L)]\right\} \\ &= \lambda\bar{\sigma}\exp(-\lambda L)\end{aligned} \quad (45)$$

Hence, substituting Equation 45 into 44 yields

$$\begin{aligned}\frac{d}{dL}[\ln(\Delta\sigma)] &= \frac{1}{\sigma_d^* + \bar{\sigma}[\exp(-\lambda L) - 1]} \\ &\quad \times \left(\frac{d\sigma_d^*}{dL} - \frac{d\sigma_{fr}}{dL}\right)\end{aligned} \quad (46)$$

It is difficult to derive a closed-form formula for the derivative of the maximum debond stress with respect to the embedded fibre length because of the complex relationship between σ_d^* and L. However, from Fig. 4 it is shown that when the embedded fibre length is shorter than the critical bonded fibre length, the slope of the σ_d^*–L curve is larger than that of the σ_{fr}–L curve. Therefore, from Equation 46 it is obtained that

$$\frac{d}{dL}[\ln(\Delta\sigma)] > 0 \qquad L < z_{max} \quad (47)$$

According to Equations 43 and 47, it can be concluded that the maximum logarithmic stress drop $\ln(\Delta\sigma)$ is obtained when the embedded fibre length is equal to the critical bonded fibre length z_{max}.

4.2. Evaluation of interfacial properties

The major objective of the micromechanics analysis for the single-fibre pull-out test is to provide a theoretical basis for experimental evaluation of the interfacial properties. Based on the above debonding and stress drop analyses, the procedure for determining the interfacial properties may be summarized as follows.

1. Determine z_{max} from the $\ln(\Delta\sigma)$ versus L curve. The stress drop data $\Delta\sigma_j$ ($j = 1$ to n) measured from single-fibre pull-out experiments for different embedded fibre length L_j can be used to calculate $\ln(\Delta\sigma_j)$ which is then plotted against L_j. The inflexion point of the experimental $\ln(\Delta\sigma_j)$ versus L_j curve is the critical bonded fibre length z_{max}.

2. Determine λ by measuring the slope of the $\ln(\Delta\sigma)$–L curve for the region $L > z_{max}$. After z_{max} is found, the stress drop data in the region $L > z_{max}$ can be used to obtain the reciprocal friction length λ which in turn is related to the frictional coefficient μ. If the slope of the $\ln(\Delta\sigma)$–L curve is $\tan\beta$ by simple linear

regression, the reciprocal friction length λ is given by

$$\lambda = -\tan\beta \tag{48}$$

and from Equation 20 the interfacial friction coefficient μ can be obtained from

$$\mu = a\lambda/2k \tag{49}$$

3. Determine $\bar{\sigma}$ from Equation 36. For the given experimental initial frictional stress data $\sigma_{fr,j}$ ($j = l$ to n) corresponding to the different embedded fibre lengths L_j there is only one unknown parameter $\bar{\sigma}$ in Equation 36 after the interfacial friction coefficient μ has been evaluated. Therefore, using a simple mean value method the asymptotic debond stress $\bar{\sigma}$ is calculated from

$$\bar{\sigma} = \frac{1}{n}\sum_{j=1}^{n}\frac{\sigma_{fr,j}}{1-\exp(-\lambda L_j)} \tag{50}$$

Hence the residual clamping stress q_0 is given from Equation 21 by

$$q_0 = -\bar{\sigma}/\omega k \tag{51}$$

4. Determine G_c from Equation 31. As in step 3, for the given experimental data $\sigma^*_{d,j}$ and L_j the interfacial fracture toughness G_c can be evaluated from

$$G_c = \frac{1}{2\pi an}\sum_{j=1}^{n}[B\sigma^{*2}_{d,j} + C(\bar{\sigma}-\sigma^*_{d,j})\sigma^*_{d,j} + D(\bar{\sigma}-\sigma^*_{d,j})^2] \tag{52}$$

where the debond lengths in the parameters B, C, and D are determined by $l_j = L_j - z_{max}$.

To illustrate the application of the present methodology, published fibre pull-out experimental data of maximum debond stress and initial frictional pull-out stress for steel wire–epoxy matrix [8, 14] and SiC fibre–glass matrix [12] composites are chosen to evaluate their interfacial properties. The material constants and geometric factors of the fibre and the matrix for the steel wire–epoxy matrix composite used in the experiments by Takaku and Arridge [14] have already been given in Table I.

Fig. 8 shows the relationship of the experimental data between the logarithmic stress drop $\ln(\Delta\sigma_j)$ and the embedded fibre length L_j for the release-agent coated steel wire–epoxy matrix [8, 14] (Fig. 8a and c), uncoated steel wire–epoxy matrix [14] (Fig. 8b) and acid-treated SiC fibre–glass matrix [12] (Fig. 8d). It is noted here and explained in Fig. 7 that if the shortest

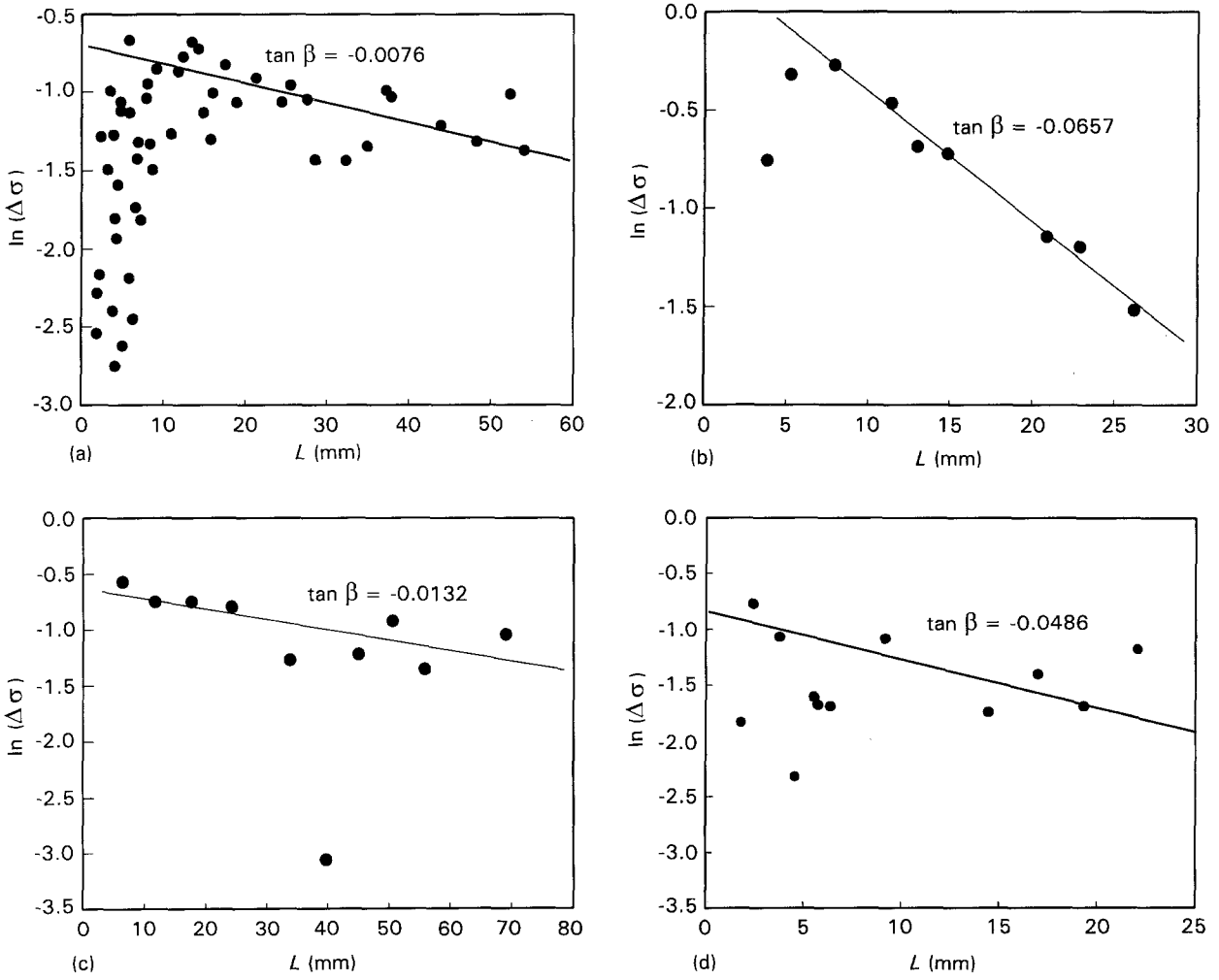

Figure 8 Experimental relationships between logarithmic stress drop $\ln(\Delta\sigma)$ and embedded fibre length L: (a) release-agent coated steel wire–epoxy matrix composite, data taken from Kim *et al.* [8]; (b) uncoated steel wire–epoxy matrix composite, data taken from Takaku and Arridge [14]; (c) release-agent coated steel wire–epoxy matrix composite, data taken from Takaku and Arridge [14]; and (d) acid-treated SiC fibre–glass matrix composite, data taken from Butler *et al.* [12].

embedded fibre length L_s used in the experiment is smaller than the critical bonded fibre length z_{max} as in Fig. 8a and b, a distinct inflexion point can be located on the $\ln(\Delta\sigma)$ versus L curve, so that an approximate z_{max} can be determined. However, if L_s is larger than z_{max} as in Fig. 8c and d, a linear experimental $\ln(\Delta\sigma)$ versus L relationship is obtained for all embedded fibre lengths, though there is a fairly large scatter for the acid-treated SiC–glass composite (Fig. 8d). In this case, a small z_{max} has to be assumed to evaluate the interfacial fracture toughness G_c. Hence, for reliable evaluation of the interfacial properties it is preferred that experimental results be obtained in the range $L < z_{max}$ in addition to $L \geq z_{max}$.

Following the steps outlined above, the interfacial properties of these fibre composites are determined and shown in Table II. Using these interfacial properties the maximum debond stress and initial frictional pull-out stress are re-calculated based on Equations 35 and 36, respectively, and are compared with experimental results in Fig. 9 for release-agent coated steel wire–epoxy matrix [8, 14] (Fig. 9a and c), uncoated steel wire–epoxy matrix [14] (Fig. 9b) and acid-treated SiC fibre–glass matrix [12] (Fig. 9d). It is obvious from these figures that the theoretical predictions (solid curves) agree well with the experimental data of the maximum debond stress and initial frictional pull-out stress. In other words, the theoretical curves plotted in Fig. 9 with the interfacial properties determined by the present methodology represent a best fit of Equation 35 to the maximum debond stress data and Equation 36 to the initial frictional pull-out stress data, respectively. This good agreement between theory and experiment has given confidence in the reliability of the interfacial properties (μ, q_0 and G_c) evaluated by the proposed methodology.

TABLE II Interfacial properties for several fibre–matrix composites

Composite system	μ	$-q_0$ (MPa)	G_c (Jm^{-2})	z_{max} (mm)
Release-agent coated steel wire–epoxy matrix [8]	0.25	6.26	65.5	8.1
Release-agent coated steel wire–epoxy [14]	0.09	13.3	54.1	2.64
Uncoated steel wire–epoxy matrix [14]	0.45	13.3	198	2.24
Acid-treated SiC fibre–glass matrix [12]	0.077	68.9	8.4	0.5

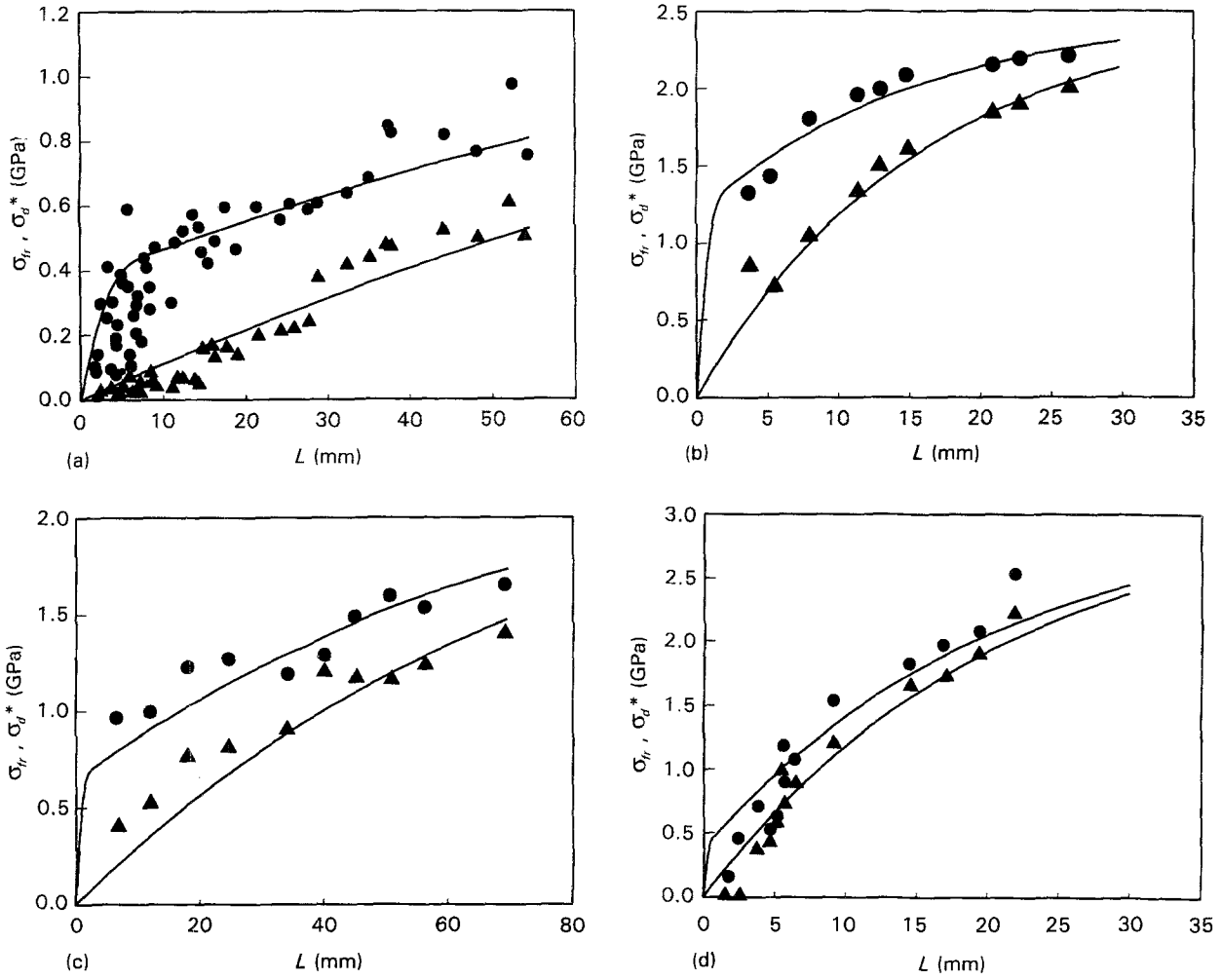

Figure 9 Comparisons between experimental results and theoretical predictions of maximum debond stress σ_d^* and initial frictional pull-out stress σ_{fr} as a function of embedded fibre length L: (a) release-agent coated steel wire–epoxy matrix composite, data taken from Kim *et al.* [8]; (b) uncoated steel wire–epoxy matrix composite, data taken from Takaku and Arridge [14]; (c) release-agent coated steel wire–epoxy matrix composite, data taken from Takaku and Arridge [14]; and (d) acid-treated SiC fibre–glass matrix composite, data taken from Butler *et al.* [12]. Experiments: (●) maximum debond stress σ_d^*, (▲) initial frictional pull-out stress σ_{fr}. Theory: (——).

5. Conclusions

A methodology for evaluation of the interfacial properties μ, q_0, G_c and z_{max} of fibre–matrix composites is proposed based on the theoretical model developed for fibre pull-out tests in Part II [9] of this paper. The stress drop ($\Delta\sigma$) analysis is presented to characterize the interface debonding instability and fibre pull-out. It is found that the maximum logarithmic stress drop $\ln(\Delta\sigma)$ is obtained when the embedded fibre length L is equal to the critical bonded fibre length z_{max} and that the slope of the $\ln(\Delta\sigma)$–L curve when $L > z_{max}$ is related to the interfacial friction coefficient μ. Applicability of the method to determine the interfacial properties of several fibre composites is demonstrated. Further, in a parametric study on a carbon fibre–epoxy matrix composite, it is shown that fibre anisotropy has a significant effect on the maximum debond and frictional pull-out stresses.

Acknowledgements

The authors wish to thank the Australian Research Council (ARC) for continuing financial support of this work. L. Ye and J. K. Kim provided many useful suggestions and stimulating discussions. LMZ is supported by both a University of Sydney Postgraduate Research Scholarship and an ARC Junior Research Fellowship.

References

1. B. BUDIANSKY, J. W. HUTCHINSON and A. G. EVANS, *J. Mech. Phys. Solids* **34** (1986) 167.
2. H. STANG and S. P. SHAH, *J. Mater. Sci.* **21** (1986) 953.
3. Y. C. GAO, Y. W. MAI and B. COTTERELL, *J. Appl. Math. Phys.* (ZAMP) **39** (1988) 550.
4. L. M. ZHOU, Y. W. MAI and Y. C. GAO, in "*Facture Mechanics of Ceramics*", Vol. 9, edited by R. C. Bradt, D. P. H. Hasselman, D. Munz and M. Sakai (Plenum, New York, 1992) p. 29.
5. J. K. KIM, L. M. ZHOU and Y. W. MAI, in "Handbook of Advanced Materials Testing", edited by N. P. Cheremisinoff (Dekker, New York, 1994) p. 327.
6. C. H. HSUEH, *Mater. Sci. Engng* **A130** (1990) L11.
7. *Idem, ibid* **A123** (1990) 1.
8. J. K. KIM, C. BAILLIE and Y. W. MAI, *J. Mater. Sci.* **27** (1992) 3143.
9. L. M. ZHOU, J. K. KIM and Y. W. MAI, *ibid.* **27** (1992) 3155.
10. J. K. KIM, L. M. ZHOU and Y. W. MAI, *ibid.* **28** (1993) 3923.
11. J. K. KIM, S. V. LU and Y. W. MAI, *ibid.* **29** (1994) p. 554.
12. E. P. BUTLER, E. R. FULLER Jr and H. M. CHAN, *Mater. Res. Soc. Symp. Proc.* **170** (1990) 17.
13. V. M. KARBHARI and D. J. WILKINS, *Scripta. Metall. Mater.* **24** (1990) 1197.
14. A. TAKAKU and R. G. C. ARRIDGE, *J. Phys. D: Appl. Phys.* **6** (1973) 2038.

Received 7 March
and accepted 22 April 1994